Adsorption and oxidation of ethanol on colloid-based Pt/C, PtRu/C and Pt_3Sn/C catalysts: *In situ* FTIR spectroscopy and on-line DEMS studies†

Q. Wang,[a] G. Q. Sun,*[a] L. H. Jiang,[ab] Q. Xin,[a] S. G. Sun,*[c] Y. X. Jiang,[c] S. P. Chen,[c] Z. Jusys[b] and R. J. Behm*[b]

Received 15th January 2007, Accepted 18th April 2007
First published as an Advance Article on the web 8th May 2007
DOI: 10.1039/b700676b

The interaction of colloid-based, carbon supported Pt/C (40 wt%), PtRu/C (45 wt%) and Pt_3Sn/C (24 wt%) catalysts with ethanol and their performance for ethanol electrooxidation were investigated in model studies by electrochemical, *in situ* infrared spectroscopy and on-line differential electrochemical mass spectrometry measurements. The combined application of *in situ* spectroscopic techniques on realistic catalysts and under realistic reaction (DEMS, IR) and transport conditions (DEMS) yields new insight on mechanistic details of the reaction on these catalysts under the above reaction and transport conditions. Based on these results, the addition of Sn or Ru, though beneficial for the overall activity for ethanol oxidation, does not enhance the activity for C–C bond breaking. Dissociative adsorption of ethanol to form CO_2 is more facile on the Pt/C catalyst than on PtRu/C and Pt_3Sn/C catalysts within the potential range of technical interests (<0.6 V), but Pt/C is rapidly blocked by an inhibiting CO adlayer. In all cases acetaldehyde and acetic acid are dominant products, CO_2 formation contributes less than 2% to the total current. The higher ethanol oxidation current density on the Pt_3Sn/C catalyst at these potentials results from higher yields of C2 products, not from an improved complete ethanol oxidation to CO_2.

1. Introduction

In the last decade, ethanol has attracted considerable interest as a fuel for direct alcohol fuel cells due to its lower toxicity and higher energy density (8.0 kW h kg^{-1}) compared with methanol.[1,2] In addition, ethanol can be easily produced in large amounts by fermentation of sugar-containing raw materials. The slow kinetics of ethanol electrooxidation at low temperatures, however, is still an obstacle for the further development of direct ethanol fuel cells (DEFCs).[3] It is well known that platinum is an active catalyst for the electrooxidation of many small organic molecules. However, at low temperatures, pure platinum is not an effective anode catalyst for ethanol electrooxidation, because it is readily poisoned by strongly adsorbed intermediates, especially by adsorbed CO.[4–13] To improve the mechanistic understanding of this complex reaction,[14] increasing attention has been paid to modern spectroscopy techniques, *e.g.*, *in situ* infrared spectroscopy (FTIR) and on-line differential electrochemical mass spectrometry (DEMS) techniques.[7,8,15] If applied, however, these spectroscopic techniques were used for model studies on massive electrodes and under idealized conditions,[4,16,17] hardly ever on supported catalysts and under more realistic reaction and transport conditions.

This is subject of the present spectro-electrochemical study, where we investigated the interaction of ethanol with carbon supported Pt/C, PtRu/C and Pt_3Sn/C catalysts by a combination of different *in situ* spectroscopic techniques, *in situ* FTIR and on-line DEMS, and electrochemical measurements under continuous reaction (DEMS, FTIR) and continuous flow (DEMS) conditions. Up to now, PtRu and Pt_3Sn have been identified as the most effective catalysts for the ethanol oxidation reaction (EOR).[13,18–21] However, only a few reports on the EOR on realistic carbon supported catalysts can be found in the literature which also include the application of spectroscopic techniques,[2,14,22–28] and especially, the role of Ru and Sn in the EOR is still not well understood. The present study provides new mechanistic insight by the combination of the above *in situ* techniques, allowing the identification of adsorbed reaction intermediates and side products and the quantitative evaluation of their coverage by *in situ* FTIR measurements as well as the determination of the (volatile) reaction products and their distribution at technically relevant potentials by on-line DEMS.

In previous *in situ* FTIR spectroscopy studies of ethanol electrooxidation on Pt or PtRu films deposited on a gold

[a] *Dalian Institute of Chemical Physics, Chinese Academy of Sciences, Dalian, 116023, Graduate School of the Chinese Academy of Sciences, Beijing, 100039, China. E-mail: gqsun@dicp.ac.cn*
[b] *Institute of Surface Chemistry and Catalysis, Ulm University, D-89069 Ulm, Germany. E-mail: juergen.behm@uni-ulm.de*
[c] *State Key Laboratory for Physical Chemistry of Solid Surfaces, Department of Chemistry, Xiamen University, Xiamen, 361005, China. E-mail: sgsun@xmu.edu.cn*

† Electronic supplementary information (ESI) available: Cyclic voltammograms of the potentiodynamic ethanol electrooxidation (Fig. S1) and polarization curves for ethanol electrooxidation on the catalysts (Fig. S2). See DOI: 10.1039/b700676b

substrate, Iwasita *et al*. determined acetaldehyde, acetic acid and CO_2 as the main products.[23,24] Variation of neither the Ru content nor the ethanol concentration led to other detectable products, but acetaldehyde was found to become increasingly dominant with increasing ethanol concentration.[24,29] Recently, it was concluded from *in situ* IR measurements that the addition of tin, *e.g*., in Pt_3Sn/C catalysts, is beneficial for the C–C bond breaking activity in ethanol oxidation and in addition offers OH species at lower potentials.[22,30,31] On the other hand, results of a recent DEMS study did not support an increased selectivity for CO_2 formation of the PtRu/C or Pt_3Sn/C catalysts compared to Pt/C.[15,25,27]

In the following we will, after a brief description of the experimental set-up and procedures used in this study, first present results on the physical characterization of the carbon supported Pt (40 wt% Pt), PtRu (30 wt% Pt, 15 wt% Ru) and Pt_3Sn (20 wt% Pt, 4 wt% Sn) catalysts by transmission electron microscopy (TEM) and X-ray diffraction (XRD) (section 3.1). This is followed by electrochemical and on-line DEMS measurements of the activity and selectivity of these catalysts towards ethanol oxidation (sections 3.2 and 3.3). The last section concentrates on the formation and identification of stable adsorbates and (volatile) reaction products upon interaction with ethanol at specific potentials (section 3.4) by electrochemical and DEMS measurements ('oxidative stripping') (section 3.4.1) and by *in situ* IR spectroscopy (section 3.4.2). The catalysts were prepared by a modified polyol method,[32] preliminary DEMS data on the EOR on similar type catalysts were reported in ref. 25.

2. Experimental

2.1 Catalyst preparation

$H_2PtCl_6 \cdot 6H_2O$, $RuCl_3 \cdot xH_2O$ and $SnCl_2 \cdot 2H_2O$ (all AR grade) were used for the synthesis of the Pt/C, PtRu/C and Pt_3Sn/C catalysts; Vulcan XC-72R carbon black (Cabot Corp., S_{BET} = 237 m^2 g^{-1}) served as support material for all samples. The required amounts of Pt, Ru and Sn compounds were added to ethylene glycol (EG) to obtain a mixture containing 2 mg metal per ml solvent. The mixture was stirred for 1/2 h at room temperature to obtain a homogeneous solution. The required amount of sodium hydroxide (1 M in EG) was added instantaneously to increase the pH value of the solution to above 13. Subsequently, the mixture was heated to 160 °C at a rate of 10 °C min^{-1} in an oil bath and kept at this temperature for 3 h. The required amount of Vulcan XC-72R was then added and the resulting mixture was stirred for another 2 h to deposit the metal particles on the support. After cooling down, the mixture was filtered to get a black filtered cake, which was washed in hot deionized water (80 °C) to remove organic residues and other ions. Then the filtered cake was dried at 80 °C for 10 h with a heating rate of about 5 °C min^{-1} in a vacuum oven. The noble metal loadings obtained for the Pt/C, PtRu/C and Pt_3Sn/C catalysts were 40 wt%, 45 wt% (nominal atomic ratio Pt : Ru = 1 : 1) and 24 wt% (nominal atomic ratio Pt : Sn = 3 : 1), respectively.

2.2 Physical characterization

XRD patterns of all samples were obtained with an X'Pert PR X-ray diffractometer using Cu Kα radiation. The 2θ angular scan was measured from 15–85° with a scan rate of 0.02° $step^{-1}$ and 10 s $step^{-1}$ (tube current 30 mA, tube voltage 40 kV). Transmission electron microscopy (TEM) was employed for the structural characterization of the catalysts, using a TECNAI F30 transmission electron microscopy (FEI Corp.).

2.3 Electrochemical and DEMS measurements

The electrochemical measurements (cyclic voltammetry (CV) and linear sweep voltammetry (LSV) measurements) were performed in a standard three-electrode RDE set-up (Pine Instruments) without rotation. A Pt foil and a saturated calomel electrode (SCE) were used as counter and reference electrodes, respectively. The preparation of the working electrodes was described previously.[32] In short, 5 mg of the respective catalyst was dispersed in a mixture of 1 ml water, 1 ml ethanol and 50 µl Nafion® solution (5 wt%) under ultrasonic stirring to form a homogeneous catalyst ink. 10 µl of this mixture was pipetted onto a polished glassy carbon (GC) disk with a diameter of 6 mm to form a homogeneous catalyst layer.

The DEMS set-up used for the electrochemical measurements and the preparation of the carbon supported Pt and Pt alloy catalyst thin film electrodes have been described in previous publications.[33–36] The DEMS set-up consists of two differentially pumped chambers, a Balzers QMS 112 quadrupole mass spectrometer, and a Pine Instruments potentiostat. In order to avoid interference with Cl^- ions, the reference electrode was separated from the main electrochemical cell by using a salt bridge containing the same solution as in the cell.

Prior to the measurements the electrode potential was scanned in the supporting electrolyte (0.5 M H_2SO_4) at a scan rate of 100 mV s^{-1} to clean the surface (from 0.06 to 1.16 V, 0.6 V, and 0.7 V for Pt/C, Pt_3Sn/C, PtRu/C, respectively). To quantify the adsorbates produced on the surface of the carbon supported Pt, Pt_3Sn and PtRu catalysts upon interaction with ethanol at different potentials, adsorbate stripping experiments were carried out after accumulation of ethanol adsorbate for a fixed time in ethanol containing electrolyte in potentiostatic measurements. The procedure of these measurements was as follows: After electrode cleaning, the electrolyte was switched from the supporting electrolyte bottle to the ethanol containing electrolyte bottle, keeping the electrode potential of 0.06 V until the baseline was stable. After that, the potential was stepped to the respective adsorption/reaction potential for 5 or 15 min to obtain (close to) steady-state currents. Then the electrolyte was switched from the ethanol-containing electrolyte back to the supporting electrolyte and, at the same time, the potential was stepped back to 0.06 V. After rinsing the cell with supporting electrolyte, the adsorbed species deposited on the surface under reaction conditions, were oxidized in a potential scan from 0.06 to 1.16 V, recording the Faradaic current and the mass spectrometric currents simultaneously. To avoid any interference between the CO_2^+ and CH_3CHO^+ ion currents (both at m/z = 44), the formation of CO_2 was monitored at m/z = 22 (CO_2^{2+}).[15,37] For

each potential studied a freshly prepared electrode was used to avoid effects resulting from EOR residues or possible losses of Sn or Ru.

2.4 *In situ* FTIR spectroscopy measurements

Electrochemical *in situ* FTIR spectroscopic studies were performed on a Nexus 870 spectrometer equipped with a liquid nitrogen cooled MCT-A detector and an EverGlo IR source, as described in ref. 38. The electrode used for the IR study was prepared in the same way as that used for the CV and LCV measurements. A CaF_2 disk was used as the IR window, and the electrode was pressed against the IR window to create a thin solution layer with a thickness of a few micrometers for *in situ* FTIR measurements. The IR radiation from the IR source passed through the CaF_2 window with an incident angle of 60° and the thin-layer solution, then reflected from the electrode surface. The spectra were collected using single potential-alteration infrared spectroscopy (SPAIRS)[39] procedures at stepwise increased potentials. At each potential, 1000 interferograms (each interferogram takes 0.46 s) at a spectral resolution of 8 cm^{-1} were co-added into a spectrum. The resulting spectrum is defined as $\Delta R/R = (R(E_S) - R(E_R))/(R(E_R) - R(E_W))$, where $R(E_S)$ and $R(E_R)$ are single-beam spectra recorded at sample potential (E_S) and reference potential (E_R), respectively. $R(E_W)$ is the single-beam spectrum of the IR window, which depends on the material and the shape of the window. Following this definition, a negative peak in the resulting spectrum represents IR absorption at E_S, equivalent to a production of species, while a positive peak signifies IR absorption at E_R and therefore consumption of the reagent. Pure N_2 and dry air (CO_2 excluded) were used to purge the electrolyte and the IR spectroscope, respectively, to reduce contributions from CO_2 and water vapor. All potentials given in this paper are referenced to that of the reversible hydrogen electrode (RHE), the measurements were performed at room temperature of around 25 ± 2 °C.

3. Results and discussion

3.1 Physical characterization of the catalysts

Fig. 1 shows TEM images of Pt/C, PtRu/C, and Pt_3Sn/C catalysts and the corresponding histograms of the particle size distribution. The metal particles, with a mean diameter of 2–3 nm, are uniformly distributed on carbon supports. From the histograms of the particle size distribution, it is clear that 90% of the particles in the Pt/C catalyst have diameters between 1.7–3.2 nm, while for the PtRu/C and Pt_3Sn/C catalysts the corresponding values are 1.2–2.7 nm. Therefore, for bimetallic catalysts there is a trend of decrease in the particle size, compared to pure Pt nanoparticles. The results suggest that the addition of Ru or Sn to Pt can reduce the agglomeration of Pt particles during the synthesis process, which was also reported in the literature.[32,40–43] The physical origin for this phenomenon, however, is still under discussion.

In the XRD patterns (Fig. 2), the diffraction peaks of the Pt/C catalyst are much sharper than those of the PtRu/C and Pt_3Sn/C catalysts, supporting the TEM based conclusion that the metal particles in the Pt/C catalyst are larger than those in the two bimetallic catalysts. A quantitative evaluation of the Pt(220) line based on the Scherrer equation yielded a mean particle size of 3.3 nm for the Pt/C catalyst; for the other two catalysts the particle size could not be evaluated because of a too low intensity of that line (PtRu/C) or because of the presence of a SnO_2 related line overlapping the Pt(220) line (Pt_3Sn/C). Only Pt diffraction peaks are observed for PtRu/C, with no indications of Ru or Ru oxides. The diffraction peaks of Pt for the PtRu/C catalyst are shifted to higher angles, indicative of PtRu alloy formation.[32] For the Pt_3Sn/C catalyst,

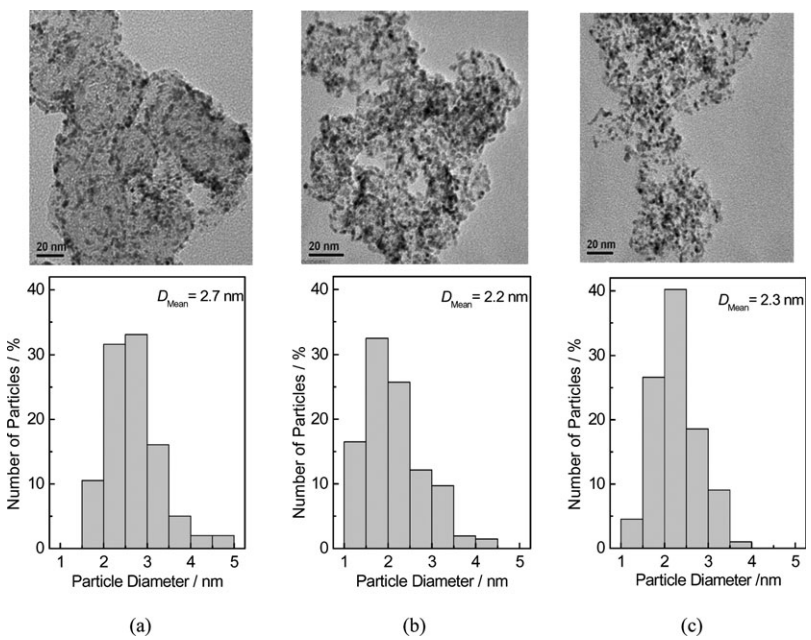

Fig. 1 TEM images and the corresponding particle size distributions of (a) Pt/C, (b) PtRu/C, (c) Pt_3Sn/C catalysts.

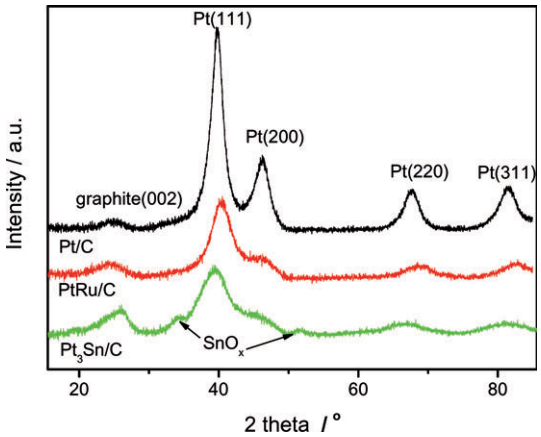

Fig. 2 X-Ray diffraction patterns of (a) Pt/C, (b) PtRu/C, (c) Pt_3Sn/C catalysts.

the Pt related diffraction peaks are shifted to lower angles, indicating Pt_3Sn alloy formation.[32,40] In addition, we observed two weak peaks for tin oxide at around 34° and 52° (PCPDF 411445),[44] which indicates that after preparation tin oxide co-exists with the Pt_3Sn alloy in the Pt_3Sn/C catalyst.[45]

3.2 Activity of Pt, PtRu, and Pt_3Sn towards ethanol electrooxidation

The activity of the three catalysts was first evaluated in CVs (see Fig. S1 in the electronic supplementary information†), together with the base CVs. The upper potential limit of the base CV and of CVs in ethanol containing electrolyte (potentiodynamic ethanol oxidation) on the PtRu/C and Pt_3Sn/C catalysts was set to 0.7 and 0.6 V, respectively, to avoid dissolution of the non-noble metal in the catalysts.[46,47] The Faradaic currents are normalized to the active surface areas, which were determined by CO_{ad} stripping[36] to be 81, 111 and 88 $m^2\ g_{metal}^{-1}$ for the Pt/C, PtRu/C and Pt_3Sn/C catalyst, respectively. The CO_{ad} stripping curves on the three catalysts are presented later in Fig. 4–6, respectively.

In these measurements the current densities at 0.6 V decrease in the order of Pt_3Sn/C > Pt/C > PtRu/C. At potentials lower than 0.57 V, this changes to Pt_3Sn/C > PtRu/C > Pt/C. The better performance of Pt/C at potentials positive to 0.6 V is ascribed to a combination of two effects, the higher efficiency of Pt for C–C bond breaking and the increased formation of OH species at these potentials which can remove the strongly adsorbed CO_{ad} species from the Pt surface. Due to the rather low upper potential limit in the scans, the curves show no distinct maximum, which based on literature reports would be expected to be around 0.8 V on PtRu/C[15,29] and 0.95 V on the Pt_3Sn/C catalyst,[2,15,32] respectively. Hydrogen adsorption is clearly inhibited on the three catalysts, indicating that the active sites of the catalysts are occupied by the reaction intermediates/side products generated from ethanol dissociation at higher potentials in the preceding negative-going scan. The identification of the adsorbed species and products will be discussed later, together with *in situ* FTIR and on-line DEMS results. In order to determine the onset potentials for ethanol electrooxidation on the different catalysts more precisely, LSV experiments were carried out at a slow scan rate of 1 mV s^{-1} on the Pt/C, PtRu/C and Pt_3Sn/C catalysts (for polarization curves see Fig. S2 in the ESI†). The profiles show that the onset of ethanol oxidation is just above 0.1 V on the Pt_3Sn/C catalyst, while on the PtRu/C and Pt/C catalysts the reaction commences at 0.3 and 0.4 V, respectively. In addition, at higher potentials (0.6–0.7 V), the EOR Faradaic current density was much higher on Pt_3Sn/C than on the other two catalysts. At potentials of technical interest, around 0.4 V, the current density on the Pt/C catalyst is negligible, while on the PtRu/C and Pt_3Sn/C catalysts it is 0.008 and 0.026 mA cm^{-2}, respectively. Thus, the Pt_3Sn/C catalyst is much more active under these conditions than the Pt/C and even the PtRu/C catalyst, with similar Pt loadings for the alloy catalysts (half of that of the Pt/C catalyst) and all catalysts prepared by the same modified polyol method. This result resembles findings by Lamy *et al.*, who reported a higher activity for Pt_xSn/C catalysts prepared *via* a co-impregnation/reduction method[14] or *via* the "Bönnemann" method[2] for ethanol oxidation than for PtRu/C and Pt/C catalysts.

3.3 Selectivity of Pt/C, Pt_3Sn/C, and PtRu/C catalysts towards the EOR

The selectivity of the Pt/C, Pt_3Sn/C, and PtRu/C catalysts in the EOR was investigated by quantitative potentiostatic electrochemical and DEMS measurements of the EOR product distribution, performed at room temperature under fuel cell relevant mass-transport and continuous reaction conditions.

Faradaic and mass spectrometric current transients, following the formation of CO_2 (m/z = 22) and acetaldehyde (m/z = 29) after a potential step from 0.06 V to the respective reaction potential, are presented in Fig. 3 (0.5 M H_2SO_4 + 0.1 M ethanol solution). For the Pt/C catalyst, we investigated reaction potentials of 0.5, 0.6, and 0.7 V. At lower potentials, the Faradaic current is negligible due to the surface poisoning by CO_{ad} resulting from the dissociative adsorption of ethanol. For the PtRu/C and Pt_3Sn/C catalysts, the lowest reaction potential could be reduced to 0.4 V due to their higher reactivity. On all three catalysts, the steady-state Faradaic current density (data obtained 15 min after the potential step) increased with potential. At technically interesting potentials lower than 0.5 V, the Faradaic current densities on Pt_3Sn/C and PtRu/C are similar, and both are distinctly higher than that on Pt/C. On the other hand, the Faradaic current density on the Pt_3Sn/C catalyst is much higher than on the PtRu/C and Pt/C catalysts at potentials of 0.5 V or above, where adsorbed residues start to be oxidized on the Pt_3Sn/C and Pt/C catalysts, and are largely oxidized on the PtRu/C catalyst (see section 3.4.1). The lower onset potential for ethanol adsorbate oxidation on the PtRu/C catalyst compared to the other catalysts indicates that PtRu/C is most efficient for adsorbate oxidation among the three catalysts. However, the Faradaic currents for the EOR on these catalysts mainly originate from the formation of C2 products rather than from complete oxidation of the adsorbates to CO_2, as evidenced by the DEMS results in section 3.4.1. The Faradaic current of the EOR on the Pt_3Sn/C catalyst is the highest for the same reason, dominant C2 formation, even though the adsorbate

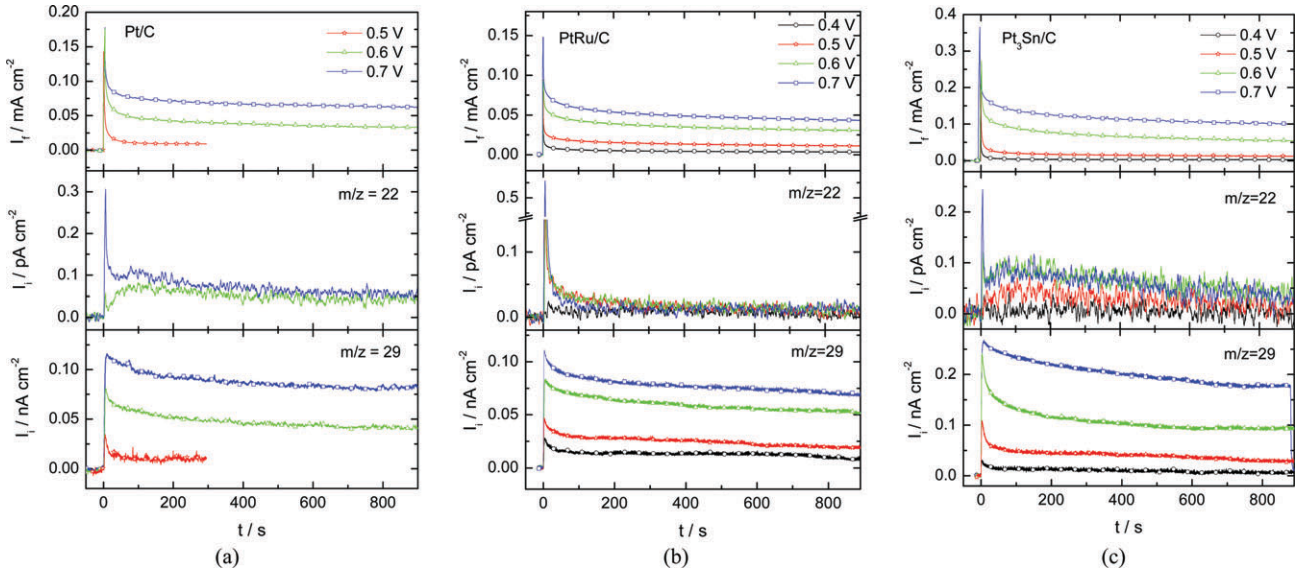

Fig. 3 Simultaneously recorded Faradaic and ion current (m/z = 22, m/z = 29) transients for ethanol oxidation on (a) Pt/C, (b) PtRu/C, and (c) Pt_3Sn/C in 0.1 M CH_3CH_2OH + 0.5 M H_2SO_4 solution at constant electrode potentials, recorded upon stepping the potential from 0.06 V to the respective reaction potential (catalyst loading: 140 μg cm^{-2}).

oxidation is not as facile as on the PtRu/C catalyst. The adsorption/dissociation of ethanol most likely occurs on Pt sites, while the second component provides OH species for CO_{ad} oxidation. Therefore, although Ru and Sn act as OH donors, the number of Pt sites at the surface, and thus dissociative adsorption, is decreased, without any improvement of the EOR selectivity for complete oxidation.

To analyze the EOR product distribution on the three catalysts in detail, the current efficiencies (A_i) and product yields (W_i) for CO_2, acetaldehyde and acetic acid formation at different potentials in 0.1 M ethanol + 0.5 M H_2SO_4 solution were calculated and listed in Table 1 (for details of the evaluation see ref. 37). At lower potentials, at 0.4 V on Pt_3Sn/C and at 0.5 V on Pt/C, the CO_2 formation rate is too low to calculate the efficiency for CO_2 formation. In general, on all three catalysts the current efficiency and product yield for CO_2 decrease with increasing potential, although the absolute amount of CO_2 formation increases slightly. Depending on the reaction potentials, the CO_2 current efficiency on these catalysts reaches at most 2% (the corresponding CO_2 yield is less than 1%). At the same potential, the current efficiency for CO_2 formation is slightly higher on the Pt_3Sn/C than on the PtRu/C catalyst, but lower than that on the Pt/C catalyst. At a potential of 0.6 V, the CO_2 current efficiencies are ~1% for Pt_3Sn/C and PtRu/C, and ~2% for Pt/C, respectively. Correspondingly, acetaldehyde and acetic acid are the majority products in the EOR within the investigated potentials. On the Pt_3Sn/C catalyst, the current efficiency for acetaldehyde formation increases with potential, while that for acetic acid decreases correspondingly, in good agreement with previous results obtained on the same catalyst in 1 M ethanol + 0.5 M H_2SO_4 solution.[25] Comparing two different ethanol concentrations (0.1 M and 1 M ethanol solution), the current efficiency and product yield for acetic acid increases with decreasing ethanol concentration (0.1 M ethanol), similar to the behavior of Pt/C.[37] This trend can be explained by the

Table 1 Faradaic currents, current efficiencies (A_i) and product yields (W_i) for CO_2, acetaldehyde and acetic acid formation during ethanol oxidation on Pt/C, PtRu/C, and Pt_3Sn/C catalysts at different potentials in 0.1 M ethanol + 0.5 M H_2SO_4 solution (data recorded 15 min after a potential step from 0.06 V to the respective reaction potential)

Catalyst	E/V *vs.* RHE	$I_{normalized}$[b]/ mA cm^{-2}	$A_i(CO_2)$ (%)	$A_i(CH_3CHO)$ (%)	$A_i(CH_3COOH)$ (%)	$W_i(CO_2)$ (%)	$W_i(CH_3CHO)$ (%)	$W_i(CH_3COOH)$ (%)
Pt_3Sn/C	0.4[a]	0.003	—	53.1	46.9	—	69.4	30.6
	0.5	0.014	2.3	46.0	51.7	1.1	63.3	35.6
	0.6	0.055	1.2	53.9	44.9	0.5	70.2	29.3
	0.7	0.080	0.8	49.7	49.5	0.4	66.5	33.1
PtRu/C	0.4[a]	0.004	1.1	41.5	57.4	0.5	58.8	40.7
	0.5	0.013	1.1	32.2	66.7	0.6	48.8	50.6
	0.6	0.030	0.8	31.7	67.5	0.4	48.2	51.4
	0.7	0.043	0.6	30.9	68.5	0.3	47.3	52.4
Pt/C	0.5	0.007[c]	—	50.0	50.0	—	66.7	33.3
	0.6	0.035	2.1	43.1	54.8	1.0	60.5	38.5
	0.7	0.060	1.5	46.4	52.1	0.7	63.6	35.7

[a] Larger error in the determination of the product distribution due to a low signal-to-noise ratio. [b] The Faradaic current is normalized by division by the active surface area S_{act} determined by CO_{ad} stripping. [c] Values obtained 5 min after the potential step to 0.5 V.

re-adsorption and further oxidation of incomplete oxidation products, which is more efficient at lower concentrations.[48] On the PtRu/C catalyst, the current efficiency for acetaldehyde decreases from 42% to 32% when the reaction potential is changed from 0.4 to 0.5 V, and then remains constant for increasing potential up to 0.7 V, which agrees closely with the trend on a similar type of 40 wt% PtRu catalyst in 1 M ethanol.[25] Also in this case, more acetic acid was formed in the 0.1 M ethanol electrolyte, which can be explained by the same 're-adsorption and oxidation' mechanism. Furthermore, more acetic acid was produced on the PtRu/C catalyst at each investigated potential than on the other catalysts (0.6 and 0.7 V: 67% current efficiency/52% product yield) (see Table 1). The higher production of acetic acid on the PtRu/C catalyst can be explained by the larger amount of available OH species on Ru sites than on Sn or Pt sites, making re-adsorption and further oxidation of acetaldehyde more effective on this catalyst than on the other ones.

3.4 Ethanol adsorbates on carbon supported Pt, PtRu, and Pt_3Sn catalysts

Topics of this section are the identification and quantification of the adsorbed decomposition products, which are produced during the interaction with ethanol under reaction conditions on the Pt/C, PtRu/C, and Pt_3Sn/C catalysts, by on-line DEMS and *in situ* FTIR techniques. It should be noted that the adsorbate coverage determined from DEMS measurements is calculated on the premise that only C1 species are adsorbed. In the FTIR measurements, approximate values of the CO_{ad} coverage are determined assuming that the CO_L intensity detected on the respective catalyst is proportional to the CO_{ad} coverage. It should be noted that CO_{ad} adsorbed on bridged and multiple sites (CO_M) have been observed upon ethanol oxidation on a Pt film electrode using *in situ* attenuated reflection Fourier transform IR spectroscopy (ATR-FTIRS) techniques,[49,50] which will contribute to the CO_{ad} coverage. These species were not observed in the present measurements, most likely because of the lower sensitivity, and therefore not included in the coverage determination.

3.4.1 DEMS measurements upon ethanol adsorption/oxidation. The coverages of the carbon containing adsorbates resulting from the dissociative adsorption of ethanol ('ethanol adsorbates') on the Pt/C, PtRu/C, and Pt_3Sn/C catalysts at specific adsorption/reaction potentials were quantified by oxidative stripping of the adsorbed species using on-line mass spectrometric detection of CO_2. The results are compared with the data from CO_{ad} stripping experiments (oxidative stripping of a pre-adsorbed CO adlayer).

The simultaneously recorded CVs and MSCVs (m/z = 22) recorded after interaction of the catalyst with ethanol at different adsorption/reaction potentials between 0.06 and 0.70 V (adsorption/reaction time: 5 min) and after pre-adsorption of CO on Pt/C, PtRu/C, and Pt_3Sn/C catalysts in 0.5 M H_2SO_4 are shown in Fig. 4–6, respectively. To evaluate the effect of the adsorption time on the adsorbate coverage for the three catalysts, similar adsorption experiments were also performed with 15 min adsorption times. Since the shapes of the CVs and MSCVs are similar in both cases, only the curves

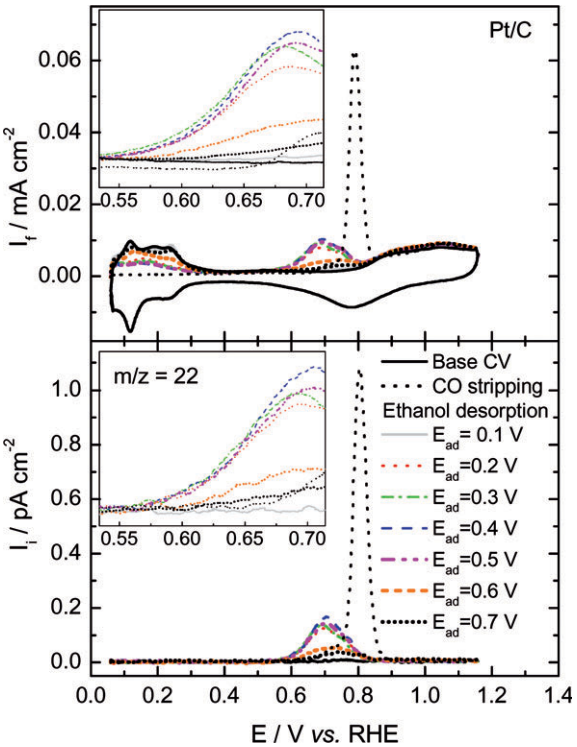

Fig. 4 CVs and MSCVs (m/z = 22) for the oxidation of ethanol adsorbates accumulated upon adsorption/reaction at different potentials (5 min) and of pre-adsorbed CO on a Pt/C catalyst in 0.5 M H_2SO_4 (catalyst loading: 140 μg cm^{-2}).

obtained after 5 min adsorption time are shown in the presentation. The oxidation of ethanol adsorbates on the Pt/C and Pt_3Sn/C catalysts occurs in two potential regions, as described in ref. 51, in the low potential region below 0.85 V and in the high potential region above 0.85 V. For the PtRu/C catalyst, these two regions are not that clearly separated. On the Pt/C and Pt_3Sn/C catalysts, the oxidation of ethanol adsorbates commences at 0.5 V and passes through a broad maximum centered at about 0.7 V, while on the PtRu/C catalyst, the oxidation of ethanol adsorbates starts at 0.3 V and peaks at 0.6 V. These results compare qualitatively with the onset potential for CO_2 formation detected in the FTIR spectra (see section 3.4.2). On all three catalysts, most of the ethanol adsorbates could be oxidized to CO_2 in the lower potential region; only a small fraction of them persists and is oxidized to CO_2 in the higher potential region.[51] In contrast, oxidation of pre-adsorbed CO (CO_{ad}) starts at 0.65, 0.4, and 0.3 V on the Pt/C, PtRu/C, and Pt_3Sn/C catalysts, respectively. Compared with the respective ignition potential for CO_{ad} oxidation, the oxidation of ethanol adsorbates starts at significantly lower potentials on the Pt/C or PtRu/C catalysts. These results agree well with observations from IR measurements on Pt film electrodes.[49,50] In contrast, on the Pt_3Sn/C catalyst, ethanol adsorbate oxidation starts at much higher potentials than the ignition potential for CO_{ad} oxidation, which is also consistent with the findings from FTIR spectroscopy (section 3.4.2).

The relative coverage of ethanol adsorbates was calculated as the ratio between the mass spectrometric charge of the

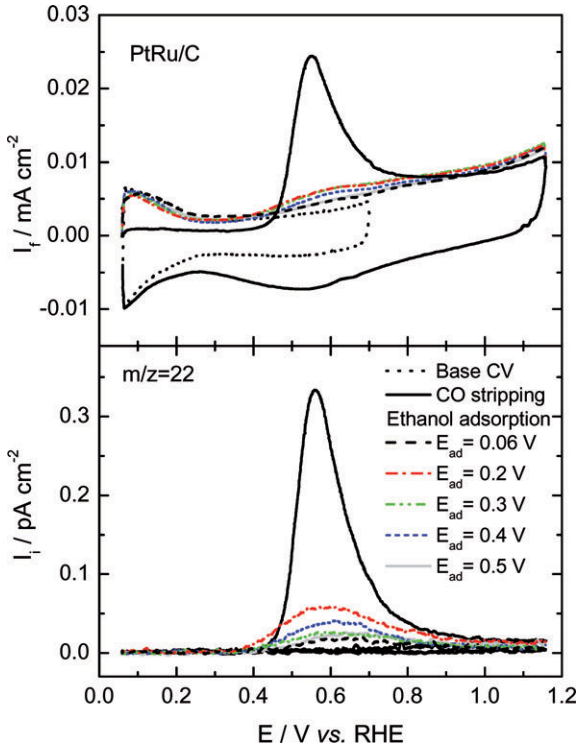

Fig. 5 CVs and MSCVs (m/z = 22) for the oxidation of ethanol adsorbates accumulated upon adsorption/reaction at different potentials (5 min) and of pre-adsorbed CO on a PtRu/C catalyst in 0.5 M H_2SO_4 (catalyst loading: 140 μg cm^{-2}).

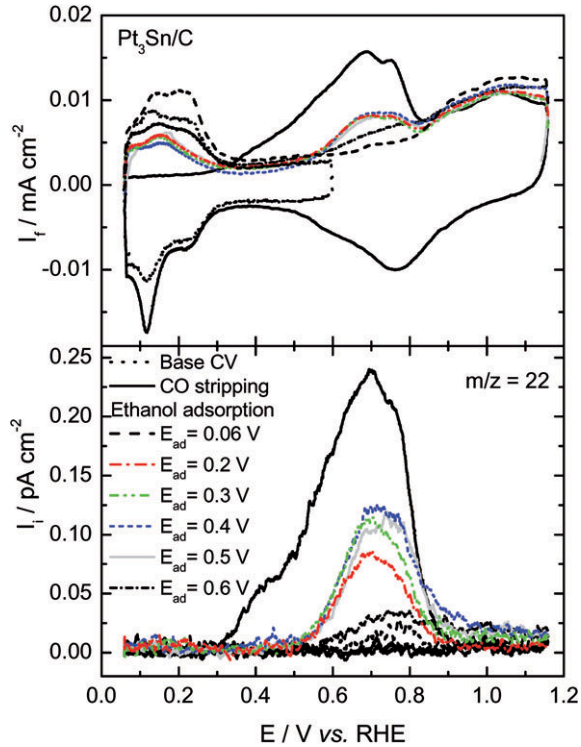

Fig. 6 CVs and MSCVs (m/z = 22) for the oxidation of ethanol adsorbates accumulated upon adsorption/reaction at different potentials (5 min) and of pre-adsorbed CO on a Pt_3Sn/C catalyst in 0.5 M H_2SO_4 (catalyst loading: 140 μg cm^{-2}).

m/z = 22 peak (CO_2^{2+}) for the oxidation of ethanol adsorbates (from Fig. 4–6) and that obtained from oxidation of a saturated CO adlayer on the respective catalyst, $\theta_{CO,sat}$ (CO adsorption at 0.06 V, m/z = 22 signal). The resulting coverages $\theta_{CO,rel}$ are shown for different adsorption potentials in Fig. 7. Note that this calculation does not correct for small amounts of adsorbed C2 species possibly present on the surface. For comparison, the relative coverage of ethanol adsorbates on a commercial 20 wt% Pt/C catalyst[51] is also plotted in Fig. 7. On all catalysts, the adsorbate coverage increases significantly when increasing the adsorption time from 5 to 15 min, indicating that ethanol adsorption is rather slow. For 15 min adsorption time, the (relative) adsorbate coverage on the 20 wt% Pt/C is comparable to that on the 40 wt% Pt/C catalyst. In addition, the potential dependence of the adsorbate uptake is similar on both Pt/C catalysts in the potential regime investigated. At the lowest adsorption potential of 0.06 V, the adsorbate coverage on the carbon supported Pt catalysts is negligible. Apparently, the relatively strong adsorption of H_{upd} almost completely inhibits the dissociative adsorption of ethanol at low potentials (<0.1 V).[51] The relative adsorbate coverage on the PtRu/C and Pt_3Sn/C catalysts at such low potentials is slightly higher than on the Pt/C catalyst, indicating that dissociative adsorption of ethanol on these two catalysts is more facile. This can be understood by the weaker and less efficient H_{upd} adsorption on the former catalysts (see Fig. S1 of the ESI†), which makes it more facile for these catalysts to (dissociatively) adsorb ethanol within the H_{upd} potential range.

Léger *et al.* also reported that the addition of Sn to Pt activates the dissociative adsorption of ethanol and the cleavage of the C–C bond at lower potentials.[30,31] However, for adsorption potentials above 0.1 V, the adsorbate coverage on Pt/C increases sharply and exceeds that on the PtRu/C and

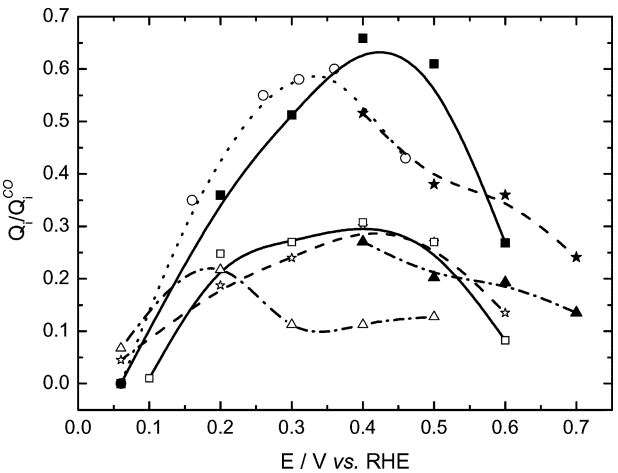

Fig. 7 Relative coverage of ethanol adsorbates compared to that of a saturated CO adlayer for different adsorption potentials on Pt/C (□ adsorption time: 5 min, ■ adsorption time: 15 min), PtRu/C (Δ: 5 min adsorption time, ▲: 15 min adsorption time), and Pt_3Sn/C (☆: 5 min adsorption time, ★: 15 min adsorption time). A commercial 20 wt% Pt/C catalyst (E-Tek) (○)[51] is included for comparison (catalyst loading: 140 μg cm^{-2}, 10 min adsorption time).

Pt_3Sn/C catalysts, achieving a maximum values of 0.28 $\theta_{CO,sat}$ and 0.63 $\theta_{CO,sat}$ at an adsorption potential of around 0.4 V after 5 min and 15 min adsorption time, respectively. On the PtRu/C and Pt_3Sn/C catalysts, maximum coverages of 0.2 $\theta_{CO,sat}$ and 0.27 $\theta_{CO,sat}$, respectively, are reached at 0.2 and 0.4 V, respectively, after 5 min adsorption time. Increasing the adsorption time to 15 min, the adsorbate coverage increases to 0.26 and 0.53 $\theta_{CO,sat}$ for the PtRu/C and Pt_3Sn/C catalysts at 0.4 V, respectively.

In total, the more facile ethanol adsorption on the bimetallic catalysts at low potentials (<0.1 V) results from the more efficient blocking of the Pt/C catalyst by H_{upd}, while at more positive potentials the higher activity of Pt for C–C bond breaking results in faster ethanol adsorption and a higher saturation coverage on the Pt/C catalyst. The ignition potentials for CO_2 formation, which are similar for Pt/C and Pt_3Sn/C, and lower for PtRu/C, reflect the lower potential for OH formation on the latter catalysts.

3.4.2 Identification of the intermediates and products by *in situ* FTIR spectroscopy. Fig. 8 shows sequences of *in situ* FTIR spectra recorded during ethanol electrooxidation on the Pt/C, PtRu/C and Pt_3Sn/C catalysts, while varying the electrode potential E_S stepwise from 0.14 to 0.84 V (reference potential 0 V). One dominant feature is a bipolar band with its negative peak at 2030 cm^{-1} and its positive peak gradually shifting to higher frequencies as E_S increases.[38,52] The bipolar band is assigned to IR absorption by linearly adsorbed CO (CO_L), produced by the dissociative adsorption of ethanol on the electrocatalyst surface. The bipolar shape results from the subtraction of the two Stark-shifted, positive CO_L bands at sample and reference potential, respectively (see section 2), which leads to a positive peak at E_R. Anomalous IR properties of CO adsorbed on nanoscale materials of noble metals, as evidenced by the positive 'absorption' peak, have been reported previously and discussed in detail by Sun's group[38,53] (see also the related discussion in ref. 54 and 55). The IR features of the CO_L bipolar band are similar on the Pt/C, PtRu/C and Pt_3Sn/C catalysts (see Fig. 8b and 8c), while the peak position and intensity vary between the catalysts due to their different adsorption properties. A negative peak (corresponding to IR absorption at E_S) near 2345 cm^{-1} is attributed to the asymmetric stretch vibration of CO_2 which appears at about 0.49 V on the Pt/C and Pt_3Sn/C catalysts, but already at 0.34 V on the PtRu/C catalyst.

Another band located at around 1715 cm^{-1}, assigned to the stretch vibration of the C=O bond in acetaldehyde and/or acetic acid as partially oxidized reaction products, appeared at a potential of about 0.49, 0.34, and 0.24 V on the Pt/C, PtRu/C, and Pt_3Sn/C catalysts, respectively, indicating that the C2 products are more easily formed on the Pt_3Sn/C catalyst than on the other ones. Actually, it is difficult to distinguish between the carbonyl groups in acetaldehyde and acetic acid, since the C=O bands in these compounds are very close, at 1713 and 1715 cm^{-1}, respectively.[7] In addition, we find four other negative bands located between 1400 and 100 cm^{-1}. For the Pt_3Sn/C catalyst, where these IR bands are strongest, they appear at 1391, 1368, 1277, and 1108 cm^{-1} at potentials higher than 0.24 V. The bands at 1391 and 1277 cm^{-1} are attributed

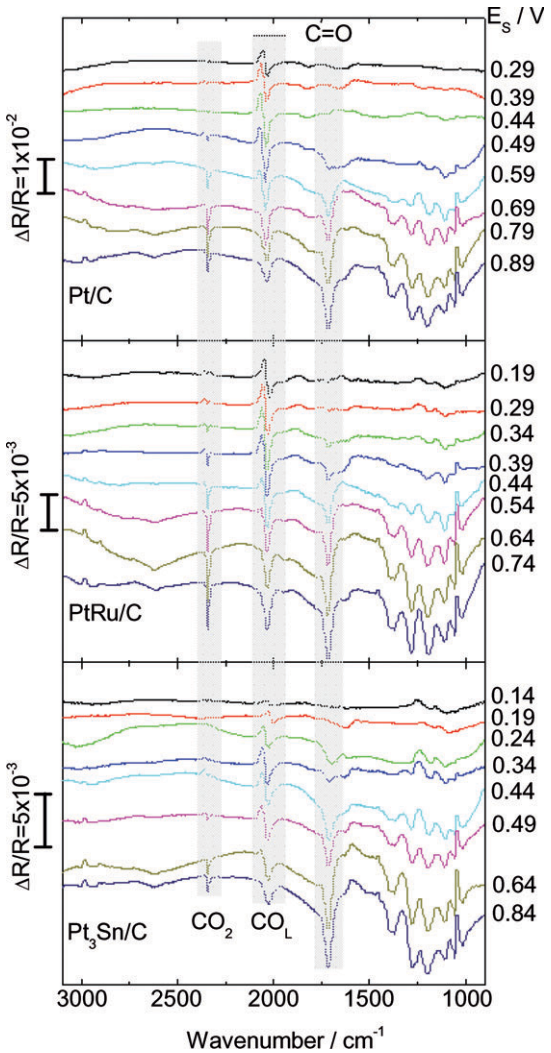

Fig. 8 *In situ* FTIR spectra recorded during ethanol electrooxidation on the (a) Pt/C, (b) PtRu/C, and (c) Pt_3Sn/C catalyst in 0.1 M H_2SO_4 + 0.1 M C_2H_5OH solution. 1000 interferograms (resolution 8 cm^{-1}) were collected and co-added into each spectrum (catalyst loading: 86 μg cm^{-2}).

to the C–O stretch and O–H deformation vibrations in acetic acid, the peaks at 1368 and 1108 cm^{-1} are due to the CH_3 symmetric deformation and C–H wagging vibration in acetaldehyde (see Table 2). At potentials above 0.49 V, a wide peak around 2622 cm^{-1} appears, which may be ascribed to an overlap of the C–H stretch (2700 to 3000 cm^{-1}) and a broad band of the O–H stretch of the carboxylic group between 2500 and 3000 cm^{-1} in acetic acid. The positive bands (corresponding to more pronounced IR absorption at E_R) at 2977 and 1455 cm^{-1} are assigned to a C–H stretch and a coupled vibration of the O–H in-plane deformation and the C–O stretch vibration in ethanol in the solution, whose intensity decays due to ethanol consumption in the thin electrolyte layer. In addition, the positive absorption band located close to 1650 cm^{-1} indicates the consumption of interfacial water. The negative peaks at 1190 and 1057 cm^{-1} can be attributed to IR absorption by adsorbed (bi-)sulfate upon CO_{ad} removal. For the Pt/C and PtRu/C catalysts, which exhibit similar

Table 2 Assignments of the fundamental bands in the spectra in Fig. 8

Wavenumber/cm^{-1}	Assignment	Ref.
2977, 2901	C–H stretching	12, 56
2062, 2030	CO_L, (C═O stretching)	12, 14, 22
2342	CO_2, asymmetric stretching	12, 14, 22
1715	C═O stretching of acetaldehyde/acetic acid	12, 14, 22
1650	O–H bending in H_2O	12, 57
1455	Coupled vibration of in plane O–H deformation and C–O stretching in C_2H_5OH	58
1391, 1277	C–O stretching and O–H deformation in CH_3COOH	2, 7, 23
1368, 1108	CH_3 symmetric deformation and C–H wagging in CH_3CHO	2, 7, 58
1190, 1057	$HSO_{4,ad}$	58

spectral features, the same assignment can be used (see compilation in Table 2).

The CO_L band intensities on the Pt/C, PtRu/C, and Pt_3Sn/C catalysts at different potentials are plotted in Fig. 9. Because of the problems in integrating the intensity of the CO_L band caused by its bipolar shape, the peak-to-peak values of the bipolar band were used instead. For comparison, the integrated intensity of the CO_2 band on the three catalysts is also included in Fig. 9. On all three catalysts, the CO_L band intensity follows a volcano-type behavior, with a low CO_L intensity at low potentials, an increase with higher potential up to a maximum value which is reached between 0.4 and 0.5 V on the Pt/C catalyst and at 0.36 V on the PtRu/C and Pt_3Sn/C catalysts, and a subsequent decay due to increasing CO_{ad} oxidation and/or decreasing CO_{ad} formation (C–C bond splitting). At each potential, the CO_L band intensity is highest on the Pt/C catalyst, indicating that C–C bond splitting is more facile and CO_{ad} is less efficiently removed on Pt/C than on the other catalysts. On the Pt/C catalyst, the resulting CO_L could only be oxidized when the potential is above 0.45 V, in contrast to the bimetallic catalysts, where, after passing the maximum at 0.36 V, the CO_L band intensity descends slowly for the PtRu/C catalyst and even slower for the Pt_3Sn/C catalyst (see also section 3.4.1). This implies that CO_L oxidation is faster on the PtRu/C catalysts than on Pt_3Sn/C at potentials higher than 0.36 V, which is also confirmed by the more pronounced increase of the CO_2 signal on the PtRu/C catalyst (see the next paragraph).

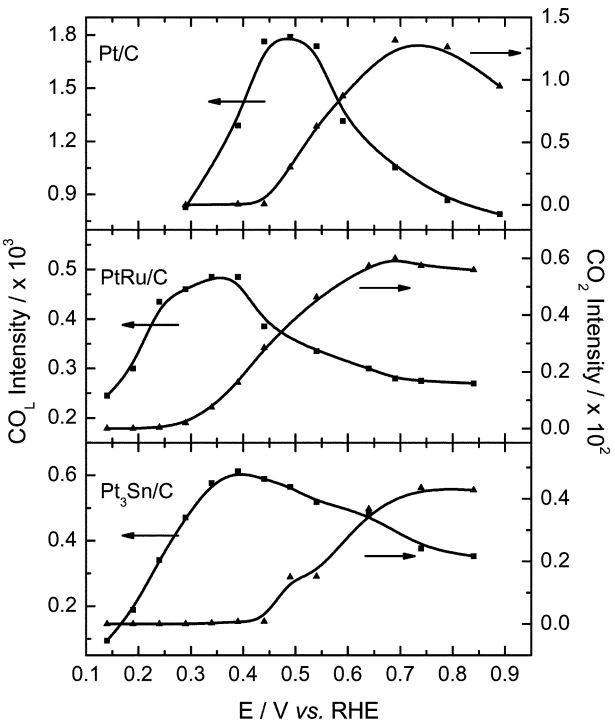

Fig. 9 IR band intensities of CO_L (peak-to-peak value in the bipolar peak) (■) and CO_2 (integrated intensity) (▲) during adsorption/oxidation of ethanol at different electrode potentials (data from Fig. 8).

Further information on the CO_{ad} oxidation behavior is obtained from the CO_2 band intensity, which during CO_{ad} oxidation increases at the expense of the CO_L intensity on the three catalysts (see Fig. 9). The formation of CO_2 commences at about 0.25 V on the PtRu/C catalyst and at 0.45 V on the Pt/C and Pt_3Sn/C catalysts, indicating that under present conditions CO_L species are more easily removed on the PtRu/C catalyst than on the other ones. This contrasts the behavior observed in CO_{ad} oxidation (CO_{ad} from CO adsorption), where CO_2 formation starts at substantially lower potential on Pt_3Sn/C than on PtRu/C or even Pt/C). One might speculate whether this is due to a different bonding situation of the CO_{ad} or whether this difference simply results from a different CO_{ad} coverage and adlayer composition obtained upon ethanol adsorption or CO adsorption. The CO_2 intensity increases with potential until 0.69 V, in good agreement with the results reported in ref. 30. For the Pt/C and PtRu/C catalysts, the CO_2 band intensity decreases slowly from 0.69 to 0.84 V, with the decay on the Pt_3Sn/C catalyst being even slower. When the potential is above 0.5 V, more CO_2 is detected over the Pt/C catalyst than over the Pt_3Sn/C catalyst at the same reaction potential. This latter result is similar to our findings from the DEMS measurements (section 3.4.1). The slight differences in the potential dependence of the adsorbate coverages derived from the DEMS and FTIR measurements are most simply explained by the differences in the experimental protocol and the transport conditions in the two types of experiments. The DEMS experiments were carried out under continuous flow conditions and at a fixed potential, starting with a freshly prepared electrode at each potential, while the IR measurements were performed in stagnant electrolyte, changing the potential stepwise to higher potentials. The different transport characteristics lead to a continuous removal of acetaldehyde and acetic acid from the electrode, while in the thin-layer IR configuration, intermediates are trapped in the catalyst layer and can be further oxidized. In addition, the metal loading in the three catalysts

also influences the intensity of the IR signals. This should lead to higher CO_2 and CO_{ad} signals for the higher loading Pt/C catalyst compared to the bimetallic catalysts, while the electrochemical and mass spectrometric signals are normalized to the active surface area, removing the loading effects.

Finally we would like to note that the intensity of the CO_L band assumes its minimum value at the same potential where the intensity of the CO_2 related band reaches its maximum, similar to reports by Léger *et al.*[30,31] This result, together with the time spent at each potential (460 s in the IR measurements), underlines that CO_2 formation is not only possible by oxidation of adsorbed CO species formed at lower potentials, but can also occur *via* dissociation and subsequent oxidation of C2 species at higher potentials, in agreement with the DEMS results presented in section 3.4.1 and ref. 51.

In total, the FTIR measurements have shown that, in addition to the strongly adsorbed CO_{ad} species and CO_2, C=O containing products are also formed in the EOR, in agreement with the DEMS results. The FTIR measurements cannot distinguish, however, between acetaldehyde or acetic acid as the two most likely candidates. The increasing formation of CO_2 correlates with a decrease in CO_L species intensity and hence in CO_L coverage. Removal of the CO_L species commences at lower potentials on the PtRu/C and Pt_3Sn/C catalysts than on the Pt/C catalyst. With increasing potential, the decay of the CO_L intensity and the increase of CO_2 intensity are less pronounced for Pt_3Sn/C than for PtRu/C, reflecting a higher activity of the PtRu/C catalyst for CO_L oxidation/CO_2 formation under these conditions. While the trends are compatible with the DEMS results presented before, a quantitative comparison between results from the two techniques has to consider the different catalysts' loadings and experimental conditions in the two types of experiments.

4. Conclusions

We have presented and discussed results of a comparative *in situ* spectro-electrochemical study on the interaction of ethanol with carbon supported Pt/C, PtRu/C and Pt_3Sn/C catalysts performed under realistic reaction conditions and under enforced electrolyte flow, *i.e.*, under controlled mass transport conditions, which allowed the identification and quantification of adsorbed reaction intermediates and products (*in situ* FTIR) and volatile reaction (side) products (on-line DEMS) on realistic catalysts and under close to realistic conditions. The measurements provide information on the nature and (potential dependent) abundance of adsorbed reaction intermediates and products, and on the nature and yields of volatile reaction products and side products, which is important for the mechanistic understanding of the EOR and the different reactions going on during the overall reaction. The catalysts were synthesized *via* a modified polyol method which results in a homogeneous distribution of the metal particles on the carbon support and very small metal particles with diameters of 2.2–2.7 nm, as derived from XRD and TEM measurements.

Information on the activity of the catalysts for the dissociative adsorption of ethanol, in particular for C–C bond breaking as a first step for ethanol oxidation, was derived from mass spectrometric ethanol adsorbate stripping experiments (detection of volatile CO_2). These measurements showed that ethanol adsorption is totally inhibited on the Pt/C catalyst at the lowest potentials investigated (0.06 V), while on PtRu/C and Pt_3Sn/C catalysts ethanol adsorption could proceed under these conditions at rather low, but non-zero rates. The complete (Pt/C) or almost complete (bimetallic catalysts) inhibition of ethanol adsorption at the lowest potential was attributed to a blocking of adsorption sites by H_{upd}, which is most strongly bound on the Pt/C catalyst, and therefore leads to the most efficient inhibition on that catalyst. At potentials above 0.1 V, however, the adsorbate coverage on the Pt/C catalyst increases sharply to exceed that on the other two catalysts, indicating that in the absence of H_{upd} dissociative ethanol adsorption is more facile on the Pt/C catalyst than on the other ones. The dissociative adsorption of ethanol results in strongly adsorbed CO_{ad} and $CH_{x,ad}$ species, which act as reaction poison for the EOR at lower potentials. There is no evidence for significant amounts of other stable adsorbates formed upon interaction with ethanol on these catalysts.

The electrocatalytic activity of the Pt_3Sn/C catalyst towards the EOR is much higher than that of the Pt/C and PtRu/C catalysts at potentials below 0.6 V. For all three catalysts and under all reaction conditions investigated, however, partial oxidation products (acetaldehyde and acetic acid) are the major EOR products, with CO_2 contributing only less than 2% of current efficiency and less than 1% of the product yield, depending on the reaction potentials and different catalysts. The higher EOR current on the Pt_3Sn/C catalyst at lower potentials is due to the higher yield of C2 products, not of CO_2. At the same reaction potential, the current efficiency (or product yield) for CO_2 formation is lowest on the PtRu/C catalyst and highest on the Pt/C catalyst.

The combined electrochemical and *in situ* spectroscopic data underlines that the current efficiency for CO_2 formation is determined by two factors, the activity for C–C bond splitting and the ability to remove the resulting CO_{ad} and $CH_{x,ad}$ species, which act as reaction poison, by oxidation. Both of these rates will depend on the potential, particularly interesting from a technical point of view are relatively low potentials (0.4–0.6 V). The resulting CO_{ad}, however, is difficult to remove from the Pt surface due to its lower oxidation activity. On the PtRu/C and Pt_3Sn/C catalysts, the dissociative adsorption of ethanol on the surface is less facile than on the Pt/C surface at these potentials, but the reaction products are oxidized faster, resulting in lower steady-state CO_{ad} coverages at the same potential and in a maximum of the steady-state CO_{ad} coverage at lower potentials compared to Pt/C. Under continuous reaction conditions at higher, but constant potentials, CO_2 formation by consumption of CO_{ad} species formed at lower potentials is not possible; the steady-state CO_2 formation rate instead reflects the oxidation of CO_{ad} and $CH_{x,ad}$ species produced at this potential.

Acknowledgements

This work was supported by the Sino-German Center at Beijing, the National Natural Science Foundation of China (Grant No. 50575036, 50676093), the Opening Foundation of the State Key Laboratory for Physical Chemistry of Solid

Surface of Xiamen University, and the Deutsche Forschungsgemeinschaft (Be 1201/12–1 and Be 1201/11–1). L. H. Jiang is grateful for a fellowship from the Alexander von Humboldt Foundation.

References

1 C. Lamy, A. Lima, V. Le Rhun, F. Delime, C. Coutanceau and J.-M. Léger, *J. Power Sources*, 2002, **105**, 283.
2 C. Lamy, S. Rousseau, E. M. Belgsir, C. Coutanceau and J.-M. Léger, *Electrochim. Acta*, 2004, **49**, 3901.
3 X. Zhao, L. H. Jiang, G. Q. Sun, S. Yang, B. Yi and Q. Xin, *Chem. J. Chin. Univ.*, 2004, **26**, 1304.
4 B. Beden, M. C. Morin, F. Hahn and C. Lamy, *J. Electroanal. Chem.*, 1987, **229**, 353.
5 P. Gao, S.-C. Chang, Z. Zhou and M. J. Weaver, *J. Electroanal. Chem.*, 1989, **272**, 161.
6 J. M. Perez, B. Beden, F. Hahn, A. Aldaz and C. Lamy, *J. Electroanal. Chem.*, 1989, **262**, 251.
7 T. Iwasita, B. Rasch and E. Cattaneo, *Electrochim. Acta*, 1989, **34**, 1073.
8 T. Iwasita and E. Pastor, *Electrochim. Acta*, 1994, **39**, 531.
9 H. Hitmi, E. M. Belgsir, J.-M. Léger, C. Lamy and R. O. Lezna, *Electrochim. Acta*, 1994, **39**, 407.
10 J. Shin, W. J. Tornquist, C. Korzeniewski and C. S. Hoaglund, *Surf. Sci.*, 1996, **364**, 122.
11 T. Iwasita, R. Dalbeck, E. Pastor and X. Xia, *Electrochim. Acta*, 1994, **39**, 1817.
12 X. H. Xia, H.-D. Liess and T. Iwasita, *J. Electroanal. Chem.*, 1997, **437**, 233.
13 F. Delime, J.-M. Léger and C. Lamy, *J. Appl. Electrochem.*, 1999, **29**, 1249.
14 F. Vigier, C. Coutanceau, A. Perrard, E. M. Belgsir and C. Lamy, *J. Appl. Electrochem.*, 2004, **34**, 439.
15 J. K. Wang, N. M. Markovic and R. R. Adzic, *J. Phys. Chem. B*, 2004, **108**, 4127.
16 V. M. Schmidt, R. Ianniello, E. Pastor and S. Gonzalez, *J. Phys. Chem.*, 1996, **100**, 17901.
17 R. Ianniello, V. M. Schmidt, J. L. Rodriguez and E. Pastor, *J. Electroanal. Chem.*, 1999, **471**, 167.
18 C. Lamy, E. M. Belgsir and J.-M. Léger, *J. Appl. Electrochem.*, 2001, **31**, 799.
19 L. Jiang, G. Sun, S. Sun, J. Liu, S. Tang, H. Li, B. Zhou and Q. Xin, *Electrochim. Acta*, 2005, **50**, 5384.
20 F. Colmati, E. Antolini and E. R. Gonzalez, *J. Power Sources*, 2006, **157**, 98.
21 X.-S. Zhao, G.-Q. Sun, L. H. Jiang, Q. Mao, Q. Xin, B.-L. Yi and S.-H. Yang, *Chem. J. Chinese Univ.*, 2005, **26**, 1304.
22 F. Vigier, C. Coutanceau, F. Hahn, E. M. Belgsir and C. Lamy, *J. Electroanal. Chem.*, 2004, **563**, 81.
23 G. A. Camara and T. Iwasita, *J. Electroanal. Chem.*, 2005, **578**, 315.
24 G. A. Camara, R. B. de Lima and T. Iwasita, *J. Electroanal. Chem.*, 2006, **585**, 128.
25 L. Colmenares, H. Wang, Z. Jusys, L. Jiang, S. Yan, G. Q. Sun and R. J. Behm, *Electrochim. Acta*, 2006, **52**, 221.
26 H. Wang, Z. Jusys and R. J. Behm, *J. Power Sources*, 2006, **154**, 351.
27 L. Jiang, L. Colmenares, Z. Jusys, G. Q. Sun and R. J. Behm, *Electrochim. Acta,* DOI: 10.1016/j.electacta.2007.01.047.
28 F. C. Simoes, D. M. dos Anjos, F. Vigier, J.-M. Léger, F. Hahn, C. Coutanceau, E. R. Gonzalez, G. Tremiliosi-Filho, A. R. de Andrade, P. Olivi and K. B. Kokoh, *J. Power Sources*, 2006, **167**, 1.
29 G. A. Camara, R. B. de Lima and T. Iwasita, *Electrochem. Commun.*, 2004, **6**, 812.
30 J.-M. Léger, S. Rousseau, C. Coutanceau, F. Hahn and C. Lamy, *Electrochim. Acta*, 2005, **50**, 5118.
31 J.-M. Léger, *Electrochim. Acta*, 2007, **50**, 3123.
32 W. Zhou, Z. Zhou, S. Song, W. Li, G. Sun, P. Tsiakaras and Q. Xin, *Appl. Catal., B*, 2003, **46**, 273.
33 T. J. Schmidt, H. A. Gasteiger, G. D. Stäb, P. M. Urban, D. M. Kolb and R. J. Behm, *J. Electrochem. Soc.*, 1998, **145**, 2354.
34 T. J. Schmidt, H. A. Gasteiger and R. J. Behm, *J. Electrochem. Soc.*, 1999, **146**, 1296.
35 Z. Jusys and R. J. Behm, *J. Phys. Chem. B*, 2001, **105**, 10874.
36 Z. Jusys, J. Kaiser and R. J. Behm, *Phys. Chem. Chem. Phys.*, 2001, **3**, 4650.
37 H. Wang, Z. Jusys and R. J. Behm, *J. Phys. Chem. B*, 2004, **108**, 19413.
38 G.-Q. Lu, S.-G. Sun, L.-R. Cai, S.-P. Chen, Z.-W. Tian and K.-K. Shiu, *Langmuir*, 2000, **16**, 778.
39 D. S. Corrigan, L.-W. H. Leung and M. J. Weaver, *Anal. Chem.*, 1987, **59**, 2252.
40 L. H. Jiang, G.-Q. Sun, Z. Zhou, W.-J. Zhou and X. Qin, *Catal. Today*, 2004, **93–95**, 665.
41 Z. Liu, X. Y. Ling, J. Y. Lee, X. Su and L. M. Gan, *J. Mater. Chem.*, 2003, **13**, 3049.
42 Z. Liu, J. Y. Lee, W. Chen, M. Han and L. M. Gan, *Langmuir*, 2004, **20**, 181.
43 W.-X. Chen, J. Y. Lee and Z. Liu, *Mater. Lett.*, 2004, **58**, 3166.
44 JCPDS, International Centre for Diffraction Data, 1987.
45 L. H. Jiang, Z. Zhou, W. Li, W.-J. Zhou, S. Somg, H.-Q. Li, G.-Q. Sun and X. Qin, *Energy Fuels*, 2004, **18**, 866.
46 C.-H. Lee, C.-W. Lee, D.-I. Kim and S.-E. Bae, *Int. J. Hydrogen Energy*, 2002, **27**, 445.
47 T. Frelink, W. Visscher and J. A. R. van Veen, *Electrochim. Acta*, 1994, **39**, 1871.
48 Z. Jusys, J. Kaiser and R. J. Behm, *Langmuir*, 2003, **19**, 6759.
49 M. H. Shao and R. R. Adzic, *Electrochim. Acta*, 2005, **50**, 2415.
50 M. Heinen, Z. Jusys, Y.-X. Chen and R. J. Behm, to be published.
51 H. Wang, Z. Jusys and R. J. Behm, *Fuel Cells*, 2004, **4**, 113.
52 Q.-S. Chen, S.-G. Sun, J.-W. Yan, J. T. Li and Z.-Y. Zhou, *Langmuir*, 2006, **22**, 10575.
53 M.-S. Zheng and S.-G. Sun, *J. Electroanal. Chem.*, 2001, **500**, 223.
54 C. Pecharroman, A. Cuesta and C. Gutiérrez, *J. Electroanal. Chem.*, 2002, **529**, 145.
55 S.-G. Sun, *J. Electroanal. Chem.*, 2002, **529**, 155.
56 A. Kabbabi, R. Faure, R. Durand, B. Beden, F. Hahn, J.-M. Léger and C. Lamy, *J. Electroanal. Chem.*, 1998, **444**, 41.
57 T. Yajima, H. Uchida and M. Watanabe, *J. Phys. Chem. B*, 2004, **108**, 2654.
58 J. G. Wu, *Modern Fourier Transform Infrared Spectroscopy Techniques and their Applications*, Scientific and Technical Document Publishing House, Beijing, 1994.

